Journal Pre-proofs

Comparison of GA and Topology Optimization of Adherend for Adhesively Bonded Metal Composite Joints

Edore G. Arhore, Mehdi Yasaee, Iman Dayyani

PII: S0020-7683(21)00168-2
DOI: https://doi.org/10.1016/j.ijsolstr.2021.111078
Reference: SAS 111078

To appear in: *International Journal of Solids and Structures*

Received Date: 4 February 2021
Revised Date: 1 April 2021
Accepted Date: 10 May 2021

Please cite this article as: Arhore, E.G., Yasaee, M., Dayyani, I., Comparison of GA and Topology Optimization of Adherend for Adhesively Bonded Metal Composite Joints, *International Journal of Solids and Structures* (2021), doi: https://doi.org/10.1016/j.ijsolstr.2021.111078

Comparison of GA and Topology Optimization of Adherend for Adhesively Bonded Metal Composite Joints

Edore G. Arhore*, Mehdi Yasaee, Iman Dayyani

School of Aerospace, Transport and Manufacturing, Cranfield MK43 0AL, UK

edore.arhore@cranfield.ac.uk

Abstract

This paper investigates the effect of the outer adherend geometry on the strength of an adhesively bonded joint. The investigation was carried out by optimizing the joint geometry using two different numerical optimization methods. In genetic algorithm (GA) optimization with high fidelity explicit finite element analysis (FEA) and topology optimization (TOP). Both procedures were utilized on a simplified pseudo-2D model as well as a full-scale 3D model. The results showed that the outer adherend geometry directly affects the strength of a joint subjected to tensile load. For joints subjected to bending load, the geometry had little to no effect on the strength of the joint. The GA optimization process produced identical geometry for both 2D and 3D models. However, the TOP process produced different optimum geometries. The optimum joints produced by the TOP process offered the highest strength overall, while the optimum GA joint produced the best strength to weight ratio. The reasons for these results and other features of the optimized designs, including interface stress, failure mechanisms and computational efficiency are discussed in detail.

Declaration of Interest: None

Keywords

Adherend, CFRP composites, adhesive joints, Abaqus, ANSYS, optimization procedure, genetic algorithm, topology optimization, MATLAB, cohesive zone modelling (CZM), continuum damage model (CDM), lightweight design

1 Introduction

The aerospace and automotive industries have a continuous aim to reduce the weight of their structures without diminishing their performance. This has led to the attraction of lightweight structures and materials which have the potential to drop structural weights by 30% [1]. Replacing conventional joining methods with adhesives provides the advantage of reduced weight and better uniform stress distribution among other benefits [2]. These advantages of adhesively bonded joints have resulted in their increased application in aerospace and automotive industries [3]. Subsequently, it has become increasingly important to develop new methods to further improve their properties.

Adhesively bonded joints can be described as the joining of multiple solid parts referred to as adherends with an adhesive [1]. There are different types of joints which include single lap, double lap, and scarf joints, among others. These joints have been characterized extensively under tension, shear and compression [4]. Some of the limitations to the application of bonded joints include the thickness and geometry of the adherends. Other limitations such as residual stress among others are outlined by Dorworth Giles Dillingham [4]. Many studies have been performed to investigate and improve adhesively bonded joint properties [5].

Studies performed by Ejaz et. al. [3], Kaye and Heller [6] and Hildebrand [7] were aimed at understanding the effect of adherend geometry on the strength of the joint. These studies were performed using non-parametric, topology, shape, and parametric optimization methods respectively. The studies were focused on tapering the edges of the adherend showing that modification of this edge directly affects the strength of the joint. Kaye and Heller [6] showed that the addition of taper allows for a better load transfer within the joint and Ejaz et. al. [3] showed that tapering the adherend edges affects the joint's stress distribution.

Investigations by Canyurt and Zhang [8] outlined that the strength of a joint is strongly dependent to the stress concentrations in the joint and that minimizing

the stress values on adhesively bonded joint results in a higher strength property. Similarly, Akpinar et al. [9] and Zhao et al. [10] showed that modifying the adherend geometry could result in better stress concentration and increased load-carrying capacity. Mitra and Ghosh [11] and Khalil et al. [12] showed that peel stress is the more dominant stress in adhesively bonded joints when compared to the shear stress. However, contradicting this, Ojalvo [13] showed that optimum joints exhibit higher shear stress values in comparison to peel stress. Results obtained by Broughton and Hinopoulos [5] and Kaye and Heller [6] showed that thickness of the adherend plays an important role, with increased adherend thickness, resulting in a reduction of the stresses acting on the joint.

Overlap length is another critical parameter that controls the strength of adhesively bonded joints, where increasing the overlap length results in an increased strength property for the joint [14] [8] [15].

Most studies performed till now have been focused on modifying single features during the optimization process. These studies have utilized different optimization methods including the parametric methods used by Hildebrand [7] and Broughton and Hinopoulos [5]. Other studies have also utilized non-parametric methods such as topology optimization which was performed by Ejaz et al. [3] and shape optimization performed by Kaye and Heller [6] and Groth and Nordlund [14]. The application of manual modification to the joint's geometry for optimization with numerical and experimental analysis has also been performed. The advantage of non-parametric methods includes the ability to explore designs that may not have previously been known [3]. However, wherewith a parametric approach, features of the design has to be studied before optimization [3].

Most of these optimization studies perform some form of numerical modelling to simulate joint designs. These numerical models can capture detailed stresses at the adherend interfaces however, in most cases, the models adopted are linear elastic or elastic-plastic simulations. None have implemented progressive damage within their models during the optimization process. Finite element (FE) analysis with cohesive zone modelling (CZM) is a useful technique to simulate

interface failure in bonded joints, which have been shown to be quite effective [2]. Although including such complex damage models within an FE framework may be computationally expensive for optimization, studies by Arhore and Yasaee [16] and Boyd et al. [17] have shown non-linear FE models implemented with optimization technique, such as genetic algorithm (GA) optimization, is feasible. Progressive damage simulation using CZM for simulating bond failure and continuum damage model (CDM) for simulating adherend failure, are useful tools available for optimization of joints and may provide new designs not previously explored.

This study aims at utilizing an optimization algorithm that will allow for a robust way of discovering the optimum geometry. This would be accomplished by allowing for a parallel modification of multiple geometric features such as the overlap length, adherend thickness and tapering of adherend edges during the optimization process. Within this process, utilization of autonomous non-linear FE models will be used to verify individual joint performance.

A tubular adhesively bonded joint comprised of a composite (IM7/8552) tube as the inner adherend and a metallic (Aluminum 7075-T6) outer adherend will be optimized. Different optimization techniques would be used to explore the vast geometric design space. The use of the different optimization techniques would allow for a comparison of the techniques via the produced optimum designs. Unique to this study is the application of advanced damage modelling techniques in plasticity, progressive failure (CDM) and CZM to simulate interface debonding with a non-linear explicit FE solver within the optimization framework. Apart from design performance, other criteria that include computational cost and efficiency will be discussed in detail.

2 Part 1: Optimization of Simplified 2D Model

2.1 Numerical Model

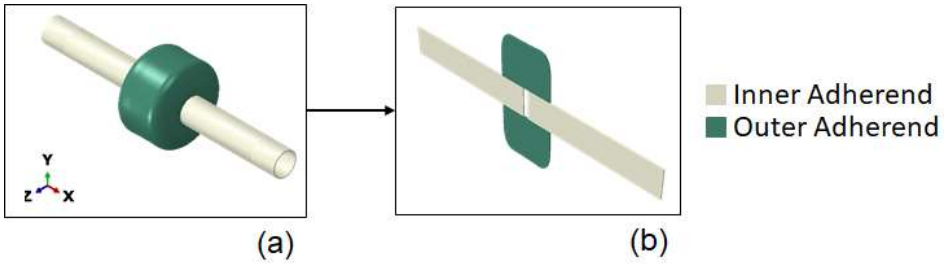

Figure 1 Planar 2D model illustration

A pseudo-2D model was used to take advantage of the key failure mechanism in of an adhesive joint. This 2D model can be described as a thin cross section cut of a full-scale 3D model targeted for optimization. Figure 1 shows an illustration of how the section cut was obtained for a sample joint model. The 2D model is composed of 4 parts which include 2 inner adherends and 2 outer adherends. The model was converted to a plain strain configuration via the application of symmetric boundary conditions to the z-faces. One advantage of using this model is its similarity with double lap strapped joints (DLSJ). This provided a good avenue for comparison with literature. The cohesive behavior between the adherends was captured using cohesive zone modelling (CZM). Continuum damage model (CDM) was used to analyze the failure of the adherends.

Table 1

Composite IM7/8552 Elastic Properties [18]

Parameter	Value
Young modulus, fiber direction (E_1)	$161GPa$
Young modulus, transverse direction (E_2, E_3)	$11.38GPa$
In-plane shear modulus (G_{12}, G_{13})	$5.17GPa$
Transverse shear Modulus (G_{23})	$3.92GPa$
Poisson's ratio (v_{12})	0.32
Poisson's ratio (v_{13})	0.32
Poisson's ratio (v_{23})	0.3813

The inner adherends were modelled as 3D deformable rectangular strips with a dimension of 50mm, 10mm and 0.5mm for the length, height, and depth

respectively. They were modelled as orthotropic laminates and assigned the elastic properties of IM7/8552 listed in Table 1. CDM was used to model the failure/damage behavior of the adherend. This was achieved by assigning the Hashin failure criteria and strength properties listed in Table 2 to the adherend. It was meshed using an 8 noded continuum shell (SC8R) element type with stacking direction set to the y axis direction (Figure 1). They were modelled as unidirectional strips to maximize tensile strength. Multiple integration points were also utilized to ensure its suitability for bending load.

The outer adherend was also modelled as 3D deformable strips. The geometry of the outer adherend was determined by the optimizer. However, the depth of the adherend was set to 0.5mm to match the depth of the inner adherend. The elastic materials properties of aluminum 7075-T6 (Table 3) were assigned to the outer adherend. The plastic and damage behavior were analyzed using CDM with the Johnson-Cook model shown in equation (1) and (2) respectively.

$$\boldsymbol{\sigma} = (\boldsymbol{A} + \boldsymbol{B}\boldsymbol{\varepsilon}^{\boldsymbol{n}})(\mathbf{1} + \boldsymbol{C}\ln\dot{\boldsymbol{\varepsilon}}^{*})(\mathbf{1} - \boldsymbol{T}^{*\boldsymbol{m}}) \quad \textbf{(1)}$$

$$\boldsymbol{\varepsilon}_{\boldsymbol{f}}^{\boldsymbol{p}} = (\boldsymbol{d}_{\mathbf{1}} + \boldsymbol{d}_{\mathbf{2}}\boldsymbol{e}^{-\boldsymbol{d}_{\mathbf{3}}\boldsymbol{\sigma}^{*}})(\mathbf{1} + \boldsymbol{d}_{\mathbf{4}}\ln\dot{\boldsymbol{\varepsilon}}^{*})(\mathbf{1} - \boldsymbol{d}_{\mathbf{5}}\boldsymbol{T}^{*}) \quad \textbf{(2)}$$

The plastic and damage parameters in these equations are listed in Table 4. The effects of temperature and strain rate were ignored during this study by setting C, d4 and d5 to 0 in equations (1) and (2).

Table 2

Composite IM7/8552 Strength Properties [18]

Parameter	Value
Tensile strength, fiber direction (X_T)	$2.3GPa$
Compressive strength, fiber direction (X_C)	$1GPa$
Tensile strength (Y_T)	$62.3MPa$
Compressive strength (Y_C)	$253.7MPa$
Shear strength (in-plane), (S_{12})	$89.6MPa$
Shear strength (S_{23})	$126.9MPa$
α	0

Table 3

Elastic Mechanical Properties of Aluminum 7075-T6 [19]

Parameter	Value
Young's modulus (E)	$71.7GPa$
Poisson's ratio (v)	0.33
Mass density (ρ)	$2810kgm^{-3}$

Table 4

Johnson-Cook Plastic and Damage Parameters of Aluminum 7075-T6 [20]

Parameter	Value
A	$473MPa$
B	$210MPa$
n	0.3813
d_1	0.3714
d_2	-0.1233
d_3	-1.9354

The adhesion between the adherends was modelled using CZM. This was done by introducing cohesive contact to the bonded surfaces. The cohesive contact was modelled with a bi-linear cohesive behavior defined with cohesive traction strength and adhesive fracture toughness. The stiffness of the cohesive contact was kept as its default value (infinitely stiff). For mixed-mode behavior, Benzeggagh-Kenane (BK) mixed-mode fracture criteria was adopted. The

cohesive damage properties for the adhesion interface are listed in Table 5. The analysis was carried out using ABAQUS explicit.

Table 5

Cohesive Damage Property [16]

Parameter	Value
G_{IC}	$210Jm^{-2}$
G_{IIC}, G_{IIIC}	$663m^{-2}$
σ_I	15
$\sigma_{II}, \sigma_{III}$	$340MPa$
$BK\ exponent$	2.1

2.2 Optimization Methodology

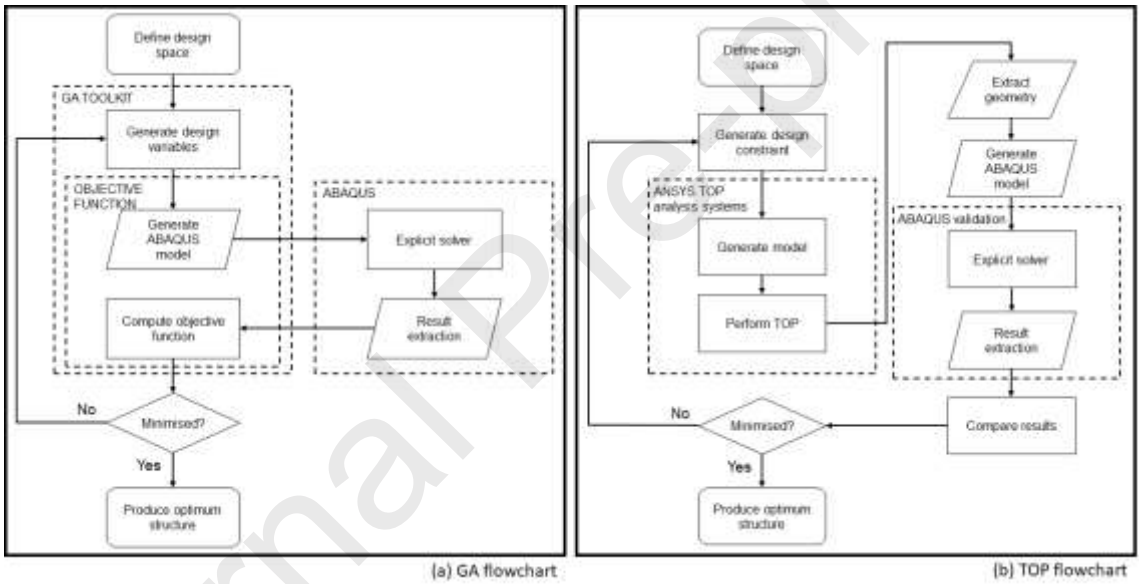

Figure 2 Optimization procedure flow chart for (a) Genetic Algorithm Optimization and (b) Topology optimization frameworks

2.2.1 Genetic Algorithm (GA) Optimization

The GA optimization toolkit in MATLAB was used to carry out the optimization process. In generating the design variables, the initial population is created randomly with a uniform distribution and restricted to specified upper and lower bounds. The algorithm then gives each population set a 'fitness value' scores based on the objective function described later. These fitness scores are then

ranked and individual sets with the best fitness values defined as ‘elite’, automatically survive to the next generation.

In the new generation, ‘Crossover’ sets are produced by a random combination of the ‘genes’ of the ‘elite’ parent sets. ‘Mutation’ sets are also created by introducing random changes, or mutations, to an ‘elite’ parent set. In this way, a children population set is generated that replaces the current parent population, forming the new generation. In the new generation, apart from the ‘elite’ children sets, the ratio of the ‘crossover’ sets to the ‘mutation’ sets is called the ‘crossover fraction’ which was set at the default of 0.8. The ‘mutation’ children set is generated by picking a random parent set and selecting the values inside the set using a Gaussian distribution.

The process of ranked scoring and generating a new generation is repeated until one of the stopping criteria is met. All other options of the GA toolkit are kept at default settings. Readers are referred to MATLAB help documents [21] and [22] which provide extensive information on the GA algorithm toolkit as well as further references on the topic.

To improve the computational time of the GA process, manual constraints could also be used to ensure only practical/feasible variables are selected in each population. For example, any variable set that does not produce a real adherend geometry is not simulated and given a penalty to be discouraged in the GA process from producing offspring.

The GA toolkit is set to maximize the objective function. As such it finds the design variables which would produce the maximum value of the objective function. For this study, the aim was to maximize the specific reaction force (SRF). The SRF was defined as the force required to completely debond the joint (RF) divided by the mass of the joint (M) as written in equation (3). The mass of the inner adherend was left constant throughout the optimization process, therefore, M could be defined as the mass of the outer adherend.

To normalize the RF and M, the min-max normalization technique equation (4) and (5) was used respectively. The min-max method can be described as a linear transformation of a data set without modifying the relationship of the data set [23]. For the implementation, the maximum value of RF (RF_{max}) was set as the force required to separate the largest possible joint design from the design space. The maximum M value (M_{max}) was measured as the mass if the entire adherend design space was filled with material. This assumption could be made as Broughton [5] has shown that thicker adherends produce stiffer joints. The minimum M value (M_{min}) was set to zero, while the minimum RF value (RF_{min}) was set to 10% of the force required to fail the inner adherend (composite beam).

$$SRF = \frac{RF_{norm}}{M_{norm}} \quad \textbf{(3)}$$

$$RF_{norm} = \frac{RF - RF_{min}}{RF_{max} - RF_{min}} \quad \textbf{(4)}$$

$$M_{norm} = \frac{M - M_{min}}{M_{max} - M_{min}} \quad \textbf{(5)}$$

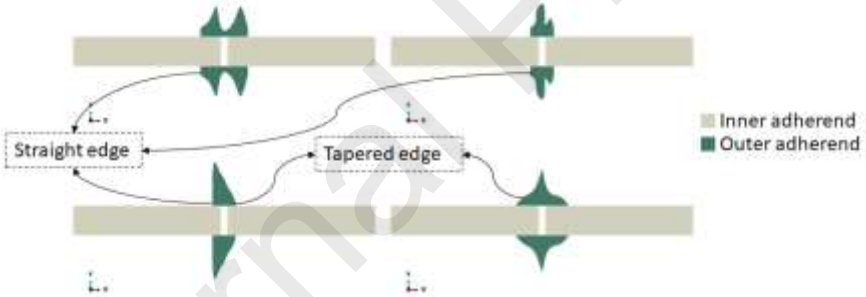

Figure 3 Illustration of some joint features produced by the optimization process

The design variable was set to define the length of the outer adherend as well as its geometric profile. The profile was modified using a spline function which was also used to modify the edges of the joint allowing for the inclusion of tapering. Figure 3 shows possible joints from the design space with different outer adherend geometry and variable overlap lengths. The figure is used to illustrate the changes in the overlap length, geometric profile, and variable edge designs. The outer adherend was mirrored about the x-axis.

As outlined by Groth and Nordlund [14], a problem associated with utilizing splines as the design variables, is the possibility of producing inappropriate sketches (example illustrated in Figure 4). These sketches would fail the numerical analysis and could terminate the entire optimization process prematurely. Therefore, it was important to ensure that errors resulting from inappropriate part design are captured not result in the termination of the entire optimization process. This was achieved by including a function to ensure the models generated were validated before FE analysis on ABAQUS.

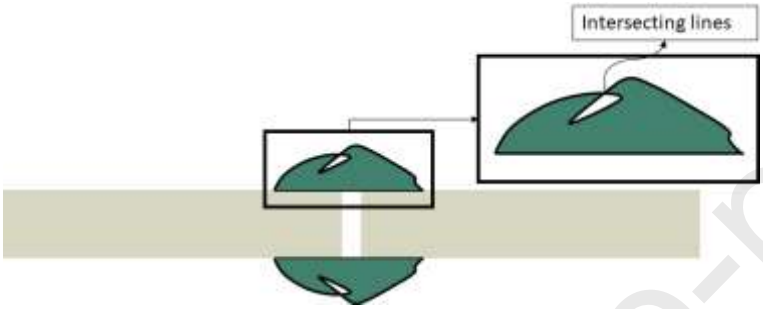

Figure 4 example of an inappropriate sketch

The flow chart of the GA optimization procedure is shown in Figure 2(a). The design variable produced by the GA toolkit autonomously generates an ABAQUS input file for validated models. All operations are conducted directly within the custom written MATLAB objective function using the MATLAB system function to execute both the ABAQUS python scripts and solver commands in Microsoft Command Prompt. In the objective function, a custom python script is written and executed using the MATLAB system function to generate the ABAQUS input file. This input file is then submitted to ABAQUS explicit solver for analysis using the MATLAB system function. A custom python script is then written autonomously by the objective function to extract the results (RF and M) of the analysis from the ABAQUS ODB output file. The SRF value was calculated using equation (3). The calculated SRF value was returned to the GA toolkit which generated a new design variable if the optimum design has not been acquired.

Although using the pseudo-2D model was aimed at minimizing computational cost. An extra measure was included to further minimize the cost. During the optimization process, it was noticed that the GA toolkit generates the design

variables from the previous generation in future generations. These designs would therefore have to be simulated multiple times producing the same results wasting computational resources. As a result, the design variables and results obtained from each iteration, during the optimization run, was recorded, and stored. This allowed the MATLAB script to return the values of design variables already simulated designs during the optimization process. This technique was noticed to reduce the overall computational cost by approximately 87%.

2.2.2 Topology Optimization (TOP) Methodology

The numerical model described in section 2.1 was maintained for the TOP analysis with few alterations. The first alteration was material properties. TOP is a linear elastic optimization procedure, therefore, only the elastic properties of the materials were assigned to the parts. The cohesive property was removed and replaced with a rigid 'tie' constraint. The TOP analysis was carried out using ANSYS. To verify the design obtained from the TOP process, the complete material and cohesive properties were assigned to the model for validation. This FEM validation step was performed using ABAQUS explicit to match the GA optimization results. The flowchart of the TOP process is shown in Figure 2(b).

An initial design was created for the optimization process. This design was set to match the upper bound of the design constraint used in the GA optimization process. The objective of the optimization was set to maximize the stiffness of the joint. The mass of the joint was used as the optimization constraint. The outer adherends were defined as the design region for the optimization process. To ensure that the inner adherend remained constant throughout the optimization process, they were defined as exclusion regions.

To ensure the results obtained from the optimization process best represented the global optimum design, the optimization process shown in Figure 2(b) was implemented. The optimization process began by performing a TOP process on the predefined joint. The optimized joint model generated was then autonomously converted to a progressive damage FE model and analyzed in ABAQUS explicit for validation of the designs in the same fashion as the GA optimization process.

The TOP procedure was repeated with a modified mass constraint value until a global optimum joint design was obtained.

2.3 Tension Load Analysis Setup and Results

Figure 5 analysis setup for tensile loading condition

The model setup used to optimize the joint subjected to tensile load is shown in Figure 5. A fully fixed boundary condition was applied to the left edge of the inner adherend. A displacement of 20mm was applied to the right edge of the inner adherend. The reaction force of the joint was measured at the edge in which the displacement was applied. For this study, the force required to completely debond the adherends was the value of interest. The objective as stated earlier was set to maximize the SRF value of the joint. However, since the inner adherends were constant, only the mass of the outer adherend would be minimized by the optimizer for a maximum SRF value.

2.3.1 Finite Element Validation and Mesh Sensitivity Test

To validate the modelling procedure described in Section 2.1, a simulation of the double lap joint experimental study performed by Campilho et al. [24] was conducted. Using the numerical modelling procedure described in section 2.1, models of the double lap joint geometry and loading with the material properties detailed in the paper [24] was generated. The mesh size used to perform the optimization process was maintained in carrying out the validation. Figure 6 compares the force-displacement graph of the model created here for validation (FEM) against the experimental and FEM results obtained from the paper [24]. A very good match between the experimental and numerical models performed in

this study is shown. This verifies that the numerical models created for this study is fully capable to capture the physical behavior of typical adhesively bonded joints.

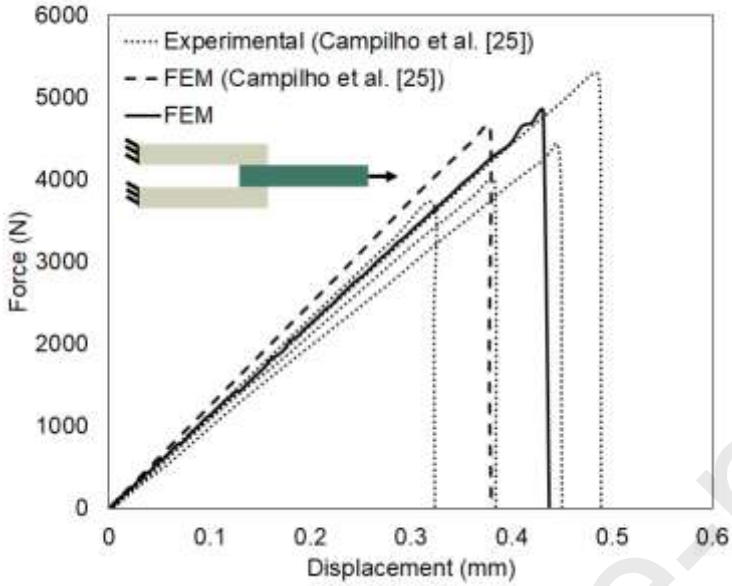

Figure 6 Validation of the numerical modelling procedure

As stated earlier, CZM was used to study the behavior of the bond between the adherends. These interface properties are dependent on mesh size. Therefore, carrying out a mesh sensitivity test was necessary. This was done to ensure that the overall behavior (response to the applied load) of the joint would not be affected by the mesh size. To minimize computational cost, it was important to use a mesh size sufficient to minimize cost without hindering the simulated behavior.

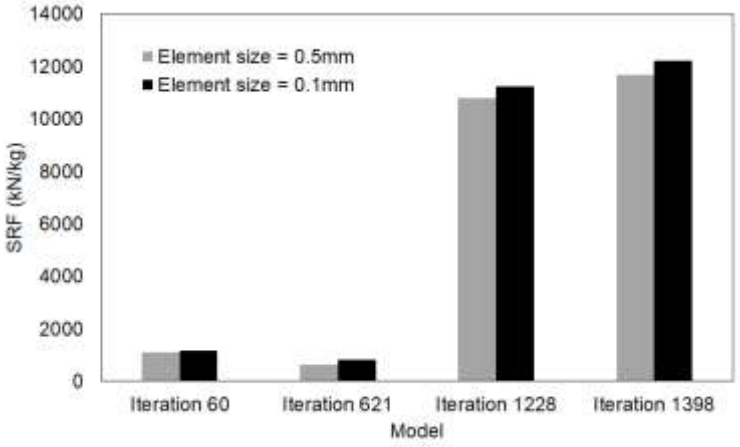

Figure 7 Effects of mesh size on the specific reaction force

The result of the sensitivity test is shown in Figure 7 for 4 randomly selected joints. As expected, reducing the mesh size increased the joint's strength. However, this behavior was seen to be uniform across all joint iterations. Therefore, it can be concluded that the mesh size would not affect the overall optimization process and result. The results also showed that the critical regions in the joint were not affected by the mesh size. Therefore, the failure mechanism (initiation region and damage progression) was unaffected by the different mesh sizes. The damage initiation regions for the joints were constant for the different mesh sizes. This is illustrated in Figure A.1 which shows the contour plot of the overall scalar damage for the cohesive surfaces indicating the adhesive failure of the bond. Figure A.2 shows the equivalent plastic strain for different mesh sizes which highlight the plastic deformation mechanism of the adherends for varying mesh sizes.

2.3.2 GA Results

The geometry of the optimum joint (GA-2DT) obtained from the optimization process is shown in Figure 8(a). The optimization process required about 14 hours for completion. The optimum edge of the outer adherend was tapered to an angle of 29^{o}. The results showed that increasing the overlap length resulted in an increased joint's strength agreeing with the findings of [14] and [15]. However, the inclusion of the joint's mass in the optimization process allowed for the production of a joint with better lightweight properties. A graph outlining the

performance of the GA optimization is shown in Figure A.3. This graph shows the maximum, average and minimum SRF value obtained for every 50 iterations (designs) produced by the GA during the optimization process.

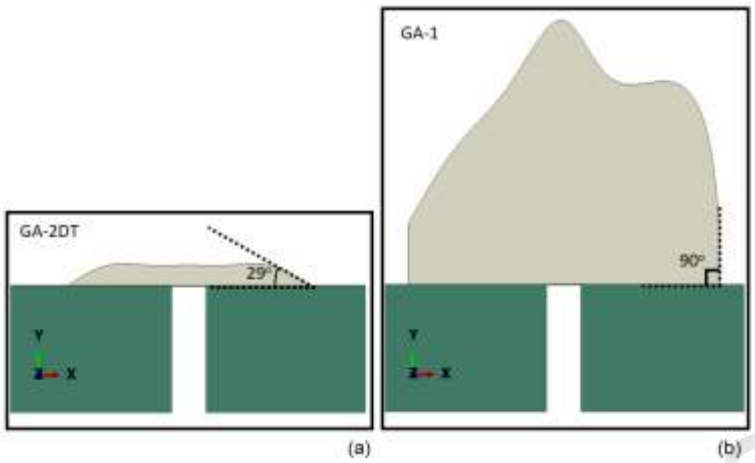

Figure 8 GA optimization process joints (a) Maximum SRF design (b) Maximum strength design

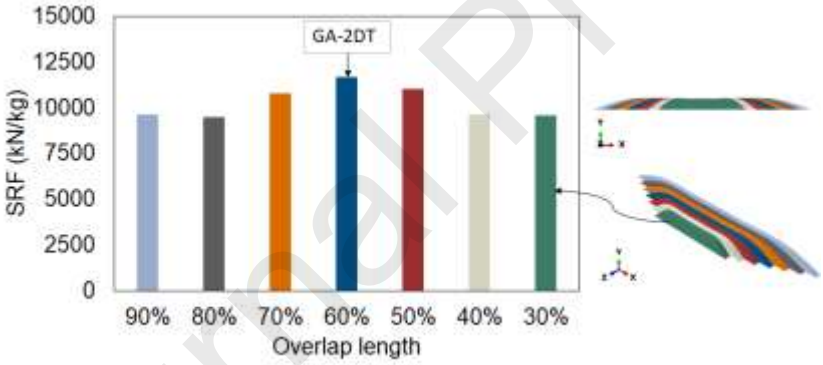

Figure 9 Effects of overlap length on the strength of the joints

Figure 9 shows the effect of the overlap length on the optimum (optimum geometric profile) joint's specific strength (SRF). Here, GA-2DT is compared with joints that exhibited the same geometric profile but a different overlap length. The SRF value peaked at an overlap length equal to 60% of the allowable length. This resulted in a weight reduction of 30% in comparison to the maximum allowable length. This result hints at the possibility of substantially reducing the weight of large-scale structures with multiple joints without degrading the structural

integrity. The results also suggested that the SRF converges to a minimum value for constant geometric profiles with increasing or reducing overlap lengths.

Figure 8(b) shows the outer adherend of a joint obtained from the optimization process labelled GA-1. The joint provided the greatest resistance to the applied load in comparison with the other generated joints. GA-1 required a load of 1.4 times that of GA-2DT for complete debonding. However, its larger mass resulted in an SRF value equal to approximately 10% of the GA-2DT value. GA-1 exhibited an overlap length of 100% of the allowable overlap length. It also exhibited a peak thickness of 130% that of GA-2DT. The higher strength of the joint could be attributed to the larger bonded region based on the results obtained by Lee [15]. Its higher strength could also be attributed to the increased thickness of the outer adherend based on the findings of Broughton [5] and Tong [25].

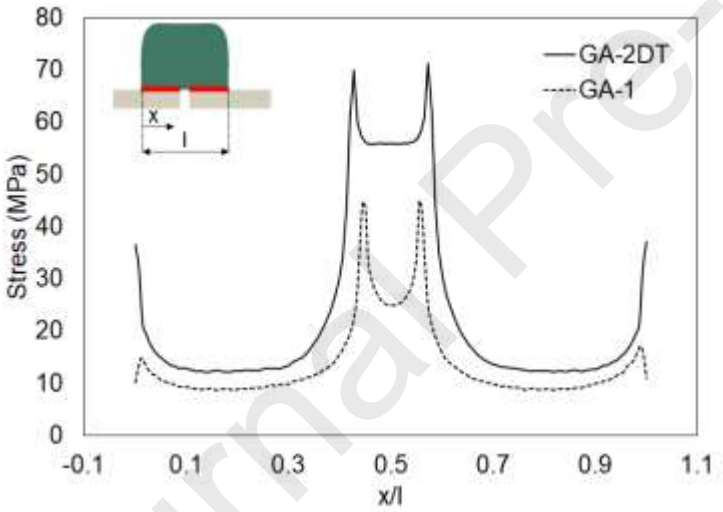

Figure 10 S11 along the bonded region of compared GA joints (2D tension)

Figure 10 shows the stress (S11) along the bonded region of the compared joints. The peak S11 values were about 4 times larger than the other stresses, establishing it as the dominating stress. Although the S11 values could not be used to accurately predict damage initiation, they provided a 100% accurate prediction for complete debonding. The results showed that joints that exhibited high S11 values would experience complete debonding first. For example, the

stress (S11) values of GA-2DT were much higher than the GA-1 joint which required a higher load for complete debonding as stated earlier.

Debonding was initiated at the edges of the GA-2DT joint which exhibited the peak stress values. The damage gradually progressed inwards from both sides of the joints. The GA-1 joint damage was initiated from the inner edges progressing outwards. An interesting behavior noticed in GA-2DT was the elastic and plastic deformation of the outer adherend. This behavior provides an extra resistance to the propagating adhesive failure and outlines the importance of high-fidelity non-linear FE analysis with progressive damage using CDM and CZM. This inclusion allowed the capture of necking in some joint designs, which dampened the debonding process improving strength. This failure mechanism cannot be captured using classical optimization processes conducted in literature and is therefore an important novelty of the procedure presented.

2.3.3 TOP Results

Figure A.4 shows the normalized SRF values for all generated geometries obtained during the optimization process with selected geometries annotated to indicate their respective SRF value. The results from the TOP process outlined the importance of using the normalization process. Without the normalization, the TOP converged to the lowest possible mass. This light joint model provided little to no resistance to the applied load. However, its small mass resulted in high SRF values producing an optimum geometry with almost zero strength. The min-max normalization method used eliminated this behavior. It also ensured that only joints which provided a minimum acceptable strength as defined in section 2.2.1 were feasible.

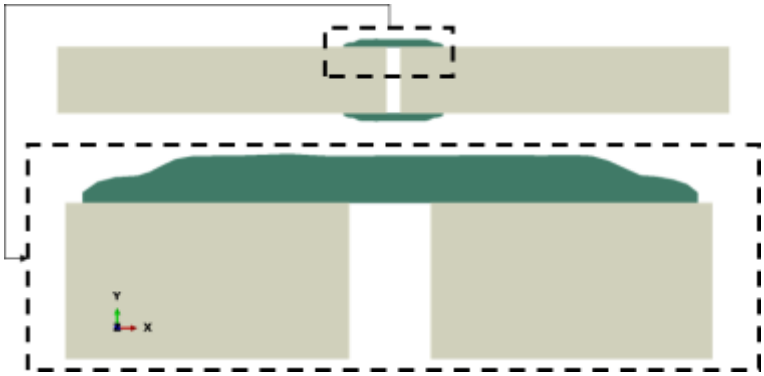

Figure 11 TOP-2DT (TOP optimized joint 2D tension)

The TOP optimized joint (TOP-2DT) obtained from the 2D optimization process is shown in Figure 11. Interestingly the edges of the outer adherend were not completely tapered, indicating that joints with straight edges can provide good strength properties. This agreed with the results obtained from the GA optimization process. The overlap length of the joint converged to a value of 65% of the allowable length which was similar to the 60% value of GA-2DT. The increased length resulted in an increased joint mass which negatively affected the SRF value. TOP-2DT produced an SRF value which was approximately 80% of the SRF value of GA-2DT.

A comparison of the S11 stress acting on the bonded region of the TOP-2DT and GA-2DT is shown in Figure 12. The results showed that both optimized joints produced a similar S11 distribution across the overlap length. This should be expected as both joints are optimum, all be it from different techniques. GA-2DT produced a slightly higher S11 peak value in the mid-region. However, the difference at the edges was more prominent with TOP-2DT exhibiting lower values. TOP-2DT produced a similar S11 distribution at the edges when compared to joints without tapered edges such as GA-1. Following the results obtained from the GA optimization analysis, it was expected that the GA-2DT would completely debond first. This is because its bonded region is subjected to higher S11 peak values. The results showed that GA-2DT does indeed produce lower maximum load compared to TOP-2DT.

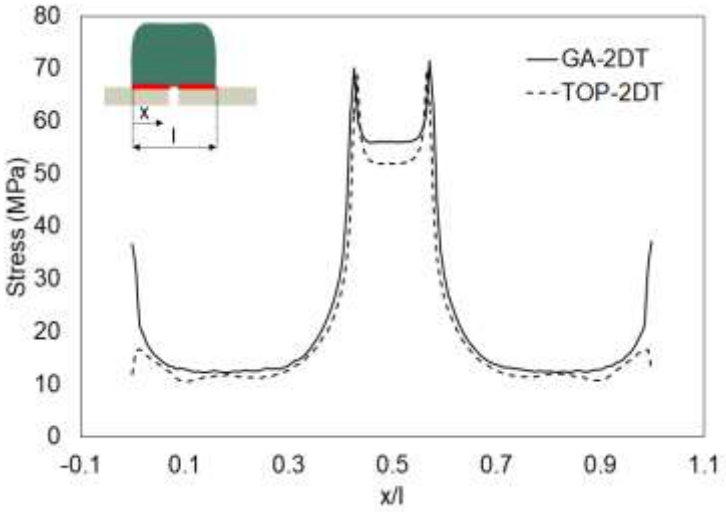

Figure 12 S11 along the bonded region of the optimized joints (2D tension)

2.4 Bending Load Analysis Setup and Results

A bending load analysis was modelled using the same setup described in Section 2.3. However, the load applied as indicated in Figure 5 was rotated by 90 degrees. The objective function, boundary condition, material properties and interaction properties described in Section 2.3 were also maintained for the analysis.

2.4.1 Results:

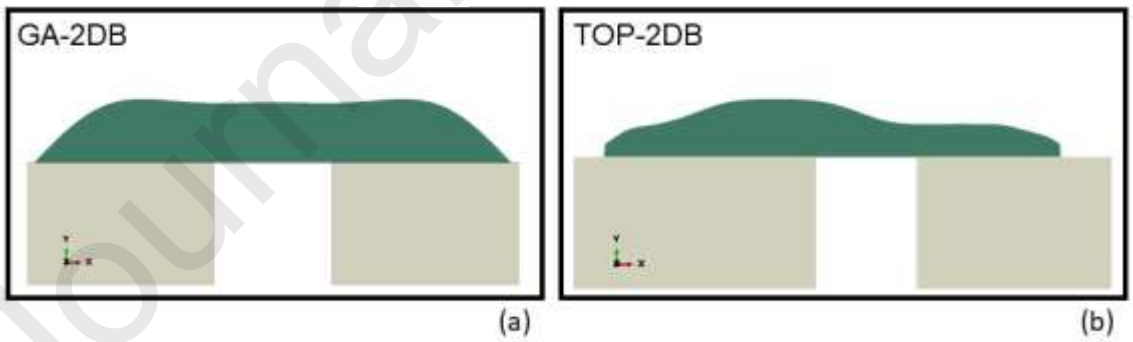

Figure 13 Optimized joint (2D bending) using (a) Genetic Algorithm optimization and (b) Topology optimization framework

The results obtained from the GA optimization process showed that the geometry of the outer adherend did not affect the strength of a joint subjected to bending load. Therefore, the GA optimizer focused on the minimization of the joint's mass. As a result, the geometry converged to the smallest allowable dimension which

failed above the minimum threshold. Figure 13(a) shows the optimized joint (GA-2DB) detailing the optimum geometry of the outer adherend.

Similarly, the TOP process converged towards the minimization of the joint's mass. However, the generated TOP optimized joint (Figure 13(b)) was not symmetric about the y-axis like the GA counterpart (Figure 13(a)). The TOP optimized joint (TOP-2DB) exhibited a thinner section at the loaded side of the outer adherend. Although this had little to no effect on the overall strength of the joint as both joints initiated and failed under similar loading conditions.

The overlap length of TOP-2DB was 18% longer than GA-2DB. However, its geometric profile resulted in it providing an equal mass property with GA-2DB. This along with the similarities with the reaction force required for complete debonding produced identical SRF values. Both joints also experienced initial debonding under the same load of 35% the load required for complete debonding. These joints also exhibited similar stress distributions. However, unlike in the case of the joints subjected to tensile load, the stress distribution was not symmetric about the x-axis.

3 Part 2: Optimization of Full-scale 3D Model

The optimized joints obtained from the 2D optimization process were modelled as tubular 3D models. The GA and TOP process described in section 2 were also used to recreate a full-scale 3D model optimization process. The purpose of this was to determine if the optimized model described in section 2 could act as a true representation of the 3D model. It also allowed for a study on the stresses acting on the 3D model and its similarity to the 2D model. Finally, this section was also aimed at measuring the effects and benefits of using a simplified model for the optimization process.

The GA 3D joint optimization process was carried out using the same procedure described previously. However, the adherends were modelled as 3D deformable revolved parts as illustrated in Figure 1(a). The material properties used for the 2D optimization process were also maintained. As before, the inner adherend

was kept constant during the optimization process. The outer adherend was modified using a spline function which was set as the design variable. The optimization process modified the joint's overlap length and the geometry of the outer adherend. The objectives of the 2D optimization process were also kept constant during the 3D optimization process.

Similarly, the TOP 3D optimization process was carried out using the same procedure used for the TOP 2D optimization. Figure 1(a) shows the initial design of the joint used for the optimization process. The design space for the optimization process was defined as the outer adherend. Although the objective function was set to maximize the stiffness of the joint, the process illustrated in Figure 2(b) was maintained. This allowed for the inclusion of CZM and CDM to obtain the global optimum joint.

3.1 Tensile Load Results

The optimized joints produced by the 3D GA optimization process was identical to the geometry of GA-2DT. The joint exhibited the same geometry including tapered edge angle, overlap length and profile. This indicates that the pseudo-2D model was indeed a good representation of the full-scale 3D model. From herein, both 3D and 2D GA optimized joints from the tension optimization process will be referred to as GA-T. The total run-time of the optimization process took approximately double the time required to complete the 2D GA optimization process. This showcases a possible saving in the computational cost by simplifying the model.

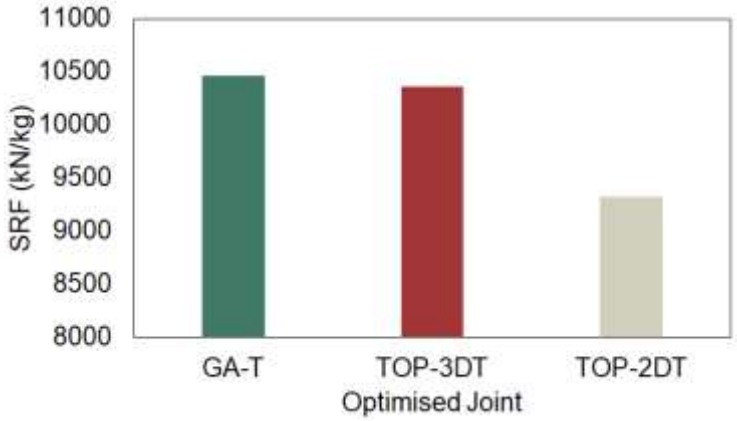

Figure 14 SRF values for the optimized joints (3D tension)

However, the 3D TOP optimized joint (TOP-3DT) did not match its 2D counterpart (TOP-2DT). TOP-3DT had an overlap length equal to 75% of the allowable length. This was 25% and 15% longer than the overlap lengths of GA-T and TOP-2DT respectively. The increased overlap length produced a better resistance to the applied load while increasing the overall mass of the joint, ultimately having a negative effect to its lightweight property. However, despite its increased mass, it still produced a high SRF value in comparison to the other joints (Figure 14).

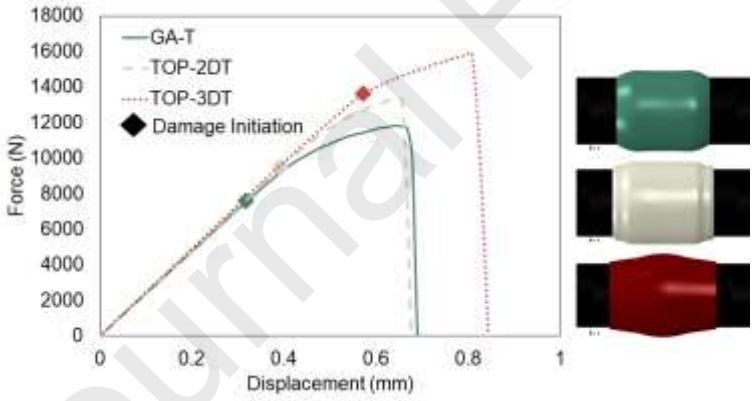

Figure 15 force-displacement graph for the optimized joints (3D tension)

Figure 15 shows the force-displacement graph for the different optimized joints. It also provides an image representation of the optimized joint. GA-T was seen to completely debond under the lowest applied load. However, its smaller mass resulted in it producing the highest SRF value (Figure 14). TOP-3DT provided the highest resistance to the applied load. However, its higher mass property negatively affected its SRF value. Despite this, it produced an SRF value which

was 98% the highest SRF value produced by GA-T. TOP-2DT also exhibited high resistance to the applied load. It outperformed GA-T in terms of load required for failure. This was similar to the results obtained from the 2D optimization process. Its high mass property, however, resulted in it exhibiting the worst lightweight property (SRF value).

Similar to the results obtained from the 2D optimization process, the stress distribution (S11) provides a method for estimating the joint's strength. Joints which exhibit higher stresses are first to completely debond. Figure 16 shows the distribution of S11 across the bonded region of the 3D optimized joints. The stress distribution was recorded at the same applied tensile load. GA-T which failed under the lowest applied load exhibited the highest S11 peak values. While TOP-3DT which required the highest load for failure exhibited the lowest S11 values. A unique difference with the planar model is that the values of S11 also accurately predicted failure initiation for all models analyzed.

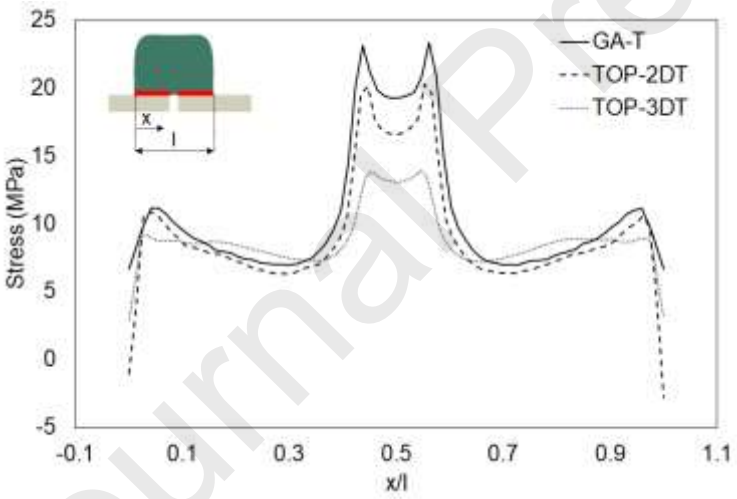

Figure 16 S11 along the bonded region of the optimized joints (3D tension)

The linear and non-linear properties of TOP-3DT also contributed to the joint's overall strength. Similar behavior was obtained during the 2D optimization process. The lighter and thinner outer adherend of the GA-2DT was noticed to undergo non-linear deformation. This provided an extra resistance to the applied load. This behavior was again noticed in GA-T and TOP-3DT which explains the higher displacements recorded on these joints (Figure 15). This deformation was

more dominant in the TOP-3DT. It resulted in its outer adherend collapsing on itself under the applied load.

3.2 Bending Load Results

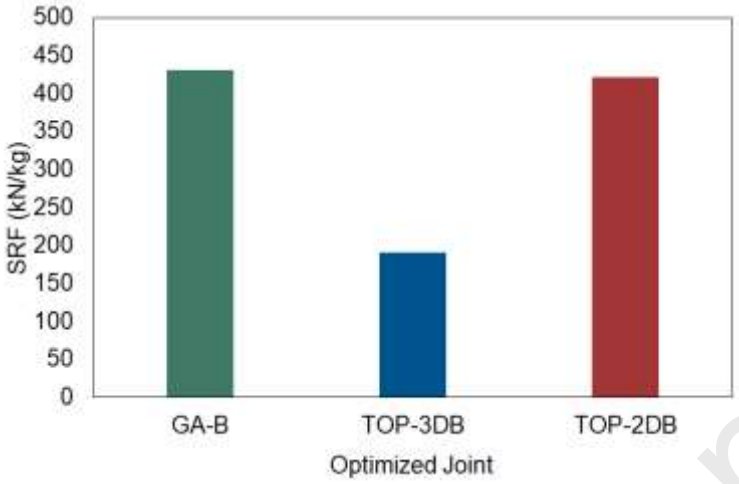

Figure 17 SRF values for the optimized joints (3D tension)

The results showed that the geometry of the outer adherend had little to no effect on the joints strength. This was similar to the results obtained from the 2D optimization process. The GA optimization process produced an optimum joint (GA-B) which matched exactly the optimum joint obtained from the 2D GA optimization process (GA-2DB). Similar to the tensile results, the 3D TOP process produced a different geometry (TOP-3DB) to TOP-2DB obtained from the 2D optimization process. In terms of computational cost, the 3D optimization process required approximately 3 times more than the 2D optimization process.

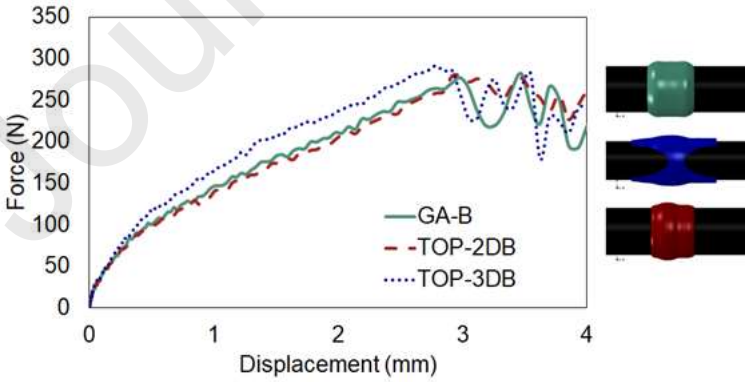

Figure 18 force-displacement graph of the optimized joints (3D tension)

Figure 18, shows the different optimized joints and the force-displacement graph. From the plots, it can be seen that GA-B and TOP-2DB reacted similarly to the applied load. However, TOP-3DB produces a different response to the applied load requiring a higher force for complete debonding. This behavioral difference can be attributed to the geometrical difference. It exhibited an outer adherend with no material at the sides. However, its large mass property resulted in the worst SRF value in comparison to the others (Figure 17).

4 Discussions and Conclusion

An investigation into the effect of the outer adherend geometry on the strength of the adhesively bonded joint was performed. The joint was comprised of composite inner adherends and metallic outer adherends. The geometry of the joint was modified using different optimization processes (GA and TOP) independently. This allowed for a comparison of different optimization processes. The optimization processes were carried out using a simplified pseudo-2D model and a full-scale 3D model.

The objective of the GA optimization process was set to maximize the strength (reaction force required to debond the adherends) while minimizing the mass of the joint. The GA optimization process produced identical geometry for the outer adherend for both the simplified 2D model and the 3D model. The results showed that the strength of the joint subjected to in-plane load was dependent on the geometry of the outer adherend. Given the identical results, the use of the simplified 2D model was able to reduce the computational cost by at least 50%. The results also showed that the strength of a joint subjected to bending load was independent of the geometry of the outer adherend allowing for the minimization of its weight.

The TOP process produced different joint geometries from the 2D and 3D optimization process. Although these joints were noticed to be stronger than the GA optimized joints, they were also heavier. This negatively affected their lightweight properties. The computational cost for the TOP process was also

similar to that of the 2D GA optimization method. The computational cost does not however include the time required to extract the geometry after the optimization process. This is because the computational cost here depends heavily on the user's skills. The requirement to extract the geometry served as a disadvantage to this method.

The results also showed that the geometry of the outer adherend affected the stress distribution along the bonded region. Joints that exhibited higher S11 distribution would completely fail first. They were also more likely to be the first to initiate failure. Although the S22 stress distribution did not accurately predict failure, it was still noticed to be geometry dependent. Thicker joints that offered higher strength overall also exhibited higher S22 values. Joints with tapered edges were also noticed to exhibit lower S22 values. The S22 values and S12 values were noticed to be inversely coupled. In order words, joints which exhibited low S22 values were more likely to exhibit higher S12 values and vice versa. Overall, joints that exhibit lower S11 distribution along the bonded region provide the greatest resistance to the applied load.

The optimization process also showcased the weight savings that could be achieved in structural joints by using optimum adherends. Although modifying the geometry of adherend affected the joints strength, minimizing the weight of the adherends did not directly weaken the joint. Therefore, the optimization process was indeed able to generate lightweight joints with good strength properties. Normalization procedure used during the optimization process was found to be very important. This is because the optimizer often preferred very small joints that produced little to no resistance to the load yet exhibited very high SRF values. The use of the min-max normalization eliminated these unrealistic joints by accepting only joints with strength values above the selected minimum.

The inclusion of plasticity and progressive damage in the optimization procedure also yielded some interesting results. The results showed that debonding of the adherend could be resisted by the non-linear behavior of the adherend. The outer adherend of GA-T was noticed to undergo necking under load application.

Although this behavior did not improve the overall strength of the joint in the 2D analysis, it did increase the strain to failure (non-brittle behavior). It also showcased the potential of capturing different behaviors, which could improve joint strength by implementing plasticity and progressive damage to the FE analysis. This potential is seen with the TOP-3DT joint in which the inclusion of the CDM allowed for the capture of it undergoing necking. This behavior was not captured during the TOP FEM analysis which was performed linearly. The results also showed that the strength of the joint was increased by this behavior. A similar result was also obtained from the analysis of the GA-T joint model in the full-scale 3D analysis, where plasticity led to improved joint strength.

Comparing the different optimization methods, the GA approach was more computationally expensive on the 2D scale. The 2D TOP process required about 80% of the computational time of the GA process. However, for the full-scale 3D optimization process, the GA process utilized less computational resources in comparison to the TOP process. The GA process also allowed for a larger design space, allowing for more geometries to be tested. It also provided a better avenue for defining the objective function. This could explain why the GA optimized joint consistently performed better in terms of producing lightweight joints. The GA optimization process also produced the same geometry as the optimized outer adherend for both the 2D and 3D analysis. This indicates that the 2D model can be used to analyze the 3D model to save computational cost in combination with the GA process.

The TOP process produced overall stronger joints; however, this came at the expense of the joint's lightweight properties. A validation step was included in the TOP process to guide the optimization process to maximize the SRF value. However, the limitation of the TOP process resulted in it, favoring the joint's strength over the weight. The TOP process did not produce uniform optimum joints for the 2D and 3D models. This indicates that the 2D model is not a true representation of the 3D model when combined with the TOP method. It is also worth noting that although the optimization processes were designed to work autonomously, the TOP process required user intervention. These interventions

included extraction of the outer adherend geometry for the FEM validation step among others and could be classified as additional computational cost and complexity.

Overall, both optimization processes exhibited both advantageous and disadvantageous characteristics. A decision matrix was used to score the performance in different classes including objective function, computational cost, modelling complexity and manufacturability among others. The GA optimization process was deemed to perform better in most of the categories. The exception was the 2D process in which the TOP process required a smaller computational cost. However, as stated earlier, the user intervention required by the TOP process could be classed as an additional computational cost.

For future studies, the GA optimization process can be modified to optimize more complex joint geometries. This could include joints with inner adherends intersecting at various angles. It could also include multiple (3 or more) intersecting inner adherends. More features could also be included such as spew fillet angle. However, increasing the complexity of the joint would increase the computational cost. As already stated, the GA method although autonomous is computationally expensive. Therefore, extra features would have to be created to minimize the possible increased cost.

The TOP process could also be modified to include a verification step similar to that included in the GA process. This could be used to check the manufacturability of the produced joint geometries. However, the most challenging aspect is setting the objective function. As stated, TOP works within the elastic region which creates a limitation to its performance. A better FEM validation could be included to alleviate this limitation, however, the requirement for human intervention could remain an issue.

References

[1] Mariam, M., Afendi, M., Abdul Majid, M. S., Ridzuan, M. J. M. and Gibson, A. G. (2018) 'Tensile and fatigue properties of single lap joints of aluminium alloy/glass fibre reinforced composites fabricated with different joining methods', *Composite Structures*. Elsevier, 200(June), pp. 647–658. Available at: https://doi.org/10.1016/j.compstruct.2018.06.003.

[2] Barbosa, N. G. C., Campilho, R. D. S. G., Silva, F. J. G. D. and Moreira, R. D. F. (2018) 'Comparison of different adhesively-bonded joint configurations for mechanical structures', *Procedia Manufacturing*. Elsevier B.V., 17, pp. 721–728. Available at: https://doi.org/10.1016/j.promfg.2018.10.122.

[3] Ejaz, H., Mubashar, A., Ashcroft, I. A., Uddin, E. and Khan, M. (2018) 'Topology optimisation of adhesive joints using non-parametric methods', *International Journal of Adhesion and Adhesives*. Elsevier Ltd, 81(October 2017), pp. 1–10. Available at: https://linkinghub.elsevier.com/retrieve/pii/S0143749617301963.

[4] Dorworth Giles Dillingham, L. C. (2017) 'Fundamentals of Adhesive Bonding of Composite Materials', in *Abaris Training*. Fort Worth.

[5] Broughton, W. R. and Hinopoulos, G. (1999) *Evaluation of the Single-Lap Joint Using Finite Element Analysis*, *NPL Report CMMT(A)*.

[6] Kaye, R. . and Heller, M. (2002) 'Through-thickness shape optimisation of bonded repairs and lap-joints', *International Journal of Adhesion and Adhesives*, 22(1), pp. 7–21. Available at: https://doi.org/10.1016/S0143-7496(01)00029-X.

[7] Hildebrand, M. (1994) 'Non-linear analysis and optimization of adhesively bonded single lap joints between fibre-reinforced plastics and metals', *International Journal of Adhesion and Adhesives*, 14(4), pp. 261–267. Available at: https://doi.org/10.1016/0143-7496(94)90039-6.

[8] Canyurt, O. E. and Zhang, J. (2006) 'Pre-stressed adhesive strap joints for thick composite sandwich structures', *International Journal of Mechanical Sciences*, 48(4), pp. 389–399. Available at: https://doi.org/10.1016/j.ijmecsci.2005.11.004.

[9] Akpinar, S., Doru, M. O., Özel, A., Aydin, M. D. and Jahanpasand, H. G. (2013) 'The effect of the spew fillet on an adhesively bonded single-lap joint subjected to bending moment', *Composites Part B: Engineering*. Elsevier Ltd, 55, pp. 55–64.

[10] Zhao, X., Adams, R. D. and da Silva, L. F. M. (2011) 'Single Lap Joints with Rounded Adherend Corners: Stress and Strain Analysis', *Journal of Adhesion Science and Technology*, 25(8), pp. 819–836. Available at: https://www.tandfonline.com/doi/full/10.1163/016942410X520871.

[11] Mitra, A. K. and Ghosh, B. (1995) 'Interfacial stresses and deformations of an adhesive bonded double strap butt joint under tension', *Computers &*

Structures, 55(4), pp. 687–694. Available at: https://doi.org/10.1016/0045-7949(94)00430-B.

[12] Khalili, S. M. R., Khalili, S., Pirouzhashemi, M. R., Shokuhfar, A. and Mittal, R. K. (2008) 'Numerical study of lap joints with composite adhesives and composite adherends subjected to in-plane and transverse loads', *International Journal of Adhesion and Adhesives*, 28(8), pp. 411–418. Available at: https://doi.org/10.1016/j.ijadhadh.2008.04.010.

[13] Ojalvo, I. (1983) 'Optimization of bonded joints', in *24th Structures, Structural Dynamics and Materials Conference*. Reston, Virigina: American Institute of Aeronautics and Astronautics. Available at: http://arc.aiaa.org/doi/10.2514/6.1983-906.

[14] Groth, H. L. and Nordlund, P. (1991) 'Shape optimization of bonded joints', *International Journal of Adhesion and Adhesives*, 11(4), pp. 204–212. Available at: https://doi.org/10.1016/0143-7496(91)90002-Y.

[15] Lee, H. K., Pyo, S. H. and Kim, B. R. (2009) 'On joint strengths, peel stresses and failure modes in adhesively bonded double-strap and supported single-lap GFRP joints', *Composite Structures*, 87(1), pp. 44–54.

[16] Arhore, E. G. and Yasaee, M. (2020) 'Lay-up optimisation of fibre–metal laminates panels for maximum impact absorption', *Journal of Composite Materials*, 54(29), pp. 4591–4609. doi: 10.1177/0021998320937396.

[17] Boyd, S. W., Blake, J. I. R., Shenoi, R. A. and Mawella, J. (2008) 'Optimisation of steel–composite connections for structural marine applications', *Composites Part B: Engineering*, 39(5), pp. 891–906. Available at: https://linkinghub.elsevier.com/retrieve/pii/S1359836807001175.

[18] Camanho, P. P. and Hallett, S. R. (2015) *Numerical Modelling of Failure in Advanced Composite Materials*. 1st edn. Woodhead Publishing.

[19] ASM Handbook Committee (1990) *Metals Handbook, Vol.2 - Properties and Selection: Nonferrous Alloys and Special-Purpose Materials, ASM International 10th Ed.* Cleveland: ASM international. Available at: http://asm.matweb.com/search/SpecificMaterial.asp?bassnum=ma7075t6 (Accessed: 29 August 2018).

[20] Zhang, D. N., Shangguan, Q. Q., Xie, C. J. and Liu, F. (2015) 'A modified Johnson-Cook model of dynamic tensile behaviors for 7075-T6 aluminum alloy', *Journal of Alloys and Compounds*. Elsevier B.V., 619, pp. 186–194.

[21] MathWorks (2020) *Find minimum of function using genetic algorithm - MATLAB ga - MathWorks United Kingdom*. Available at: https://uk.mathworks.com/help/gads/ga.html (Accessed: 13 May 2020).

[22] MathWorks (2020) *How the Genetic Algorithm Works - MATLAB & Simulink - MathWorks United Kingdom*. Available at: https://uk.mathworks.com/help/gads/how-the-genetic-algorithm-works.html (Accessed: 13 May 2020).

[23] Han, J., Kamber, M. and Pei, J. (2012) 'Data Preprocessing', in *Data Mining*.

Elsevier, pp. 83–124. Available at: https://doi.org/10.1016/B978-0-12-381479-1.00003-4.

[24] Campilho, R. D. S. G., Banea, M. D., Pinto, A. M. G., da Silva, L. F. M. and de Jesus, A. M. P. (2011) 'Strength prediction of single- and double-lap joints by standard and extended finite element modelling', *International Journal of Adhesion and Adhesives*. Elsevier, 31(5), pp. 363–372. doi: 10.1016/j.ijadhadh.2010.09.008.

[25] Tong, L. (1994) 'Bond shear strength for adhesive bonded double-lap joints', *International Journal of Solids and Structures*. Elsevier Science Ltd., 31(21), pp. 2919–2931. Available at: http://dx.doi.org/10.1016/0020-7683(94)90059-0.

Appendix 1

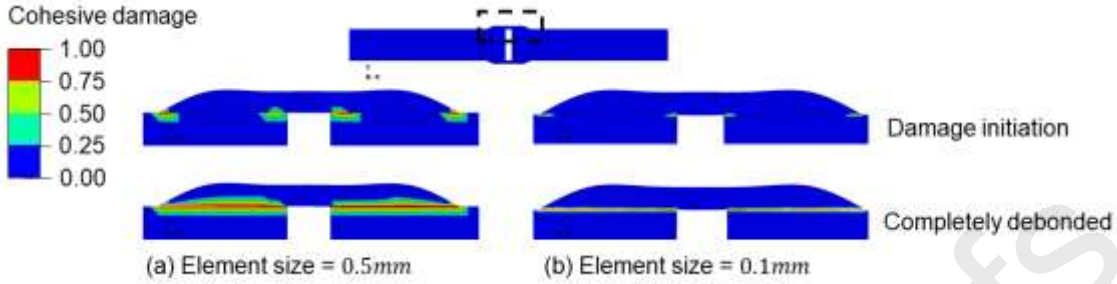

Figure A.1 Effect of mesh size on cohesive damage

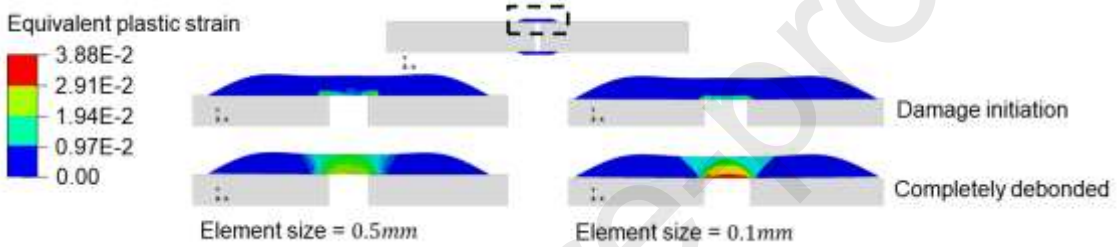

Figure A.2 Effect of mesh size equivalent plastic strain

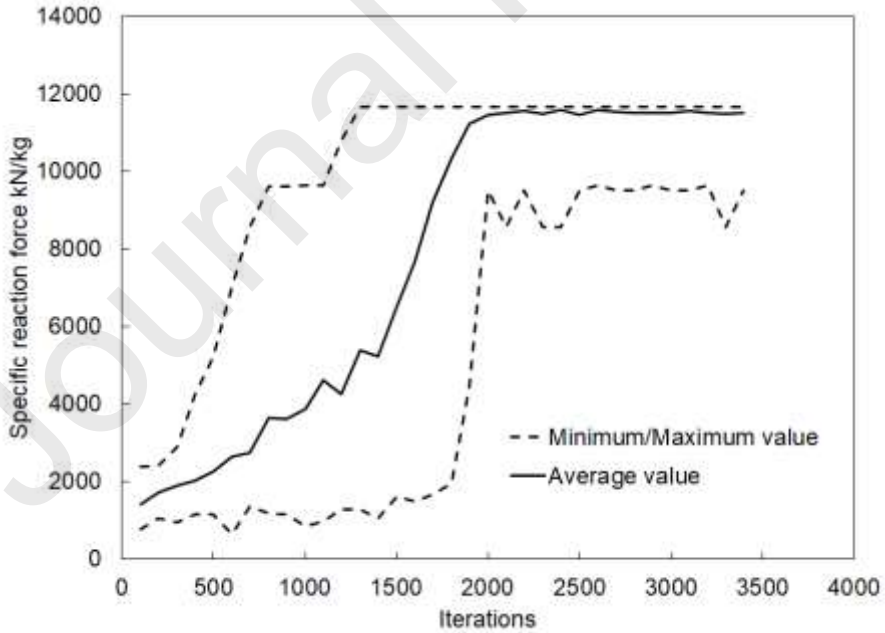

Figure A.3 Performance of GA optimization process averaged every 50 iterations

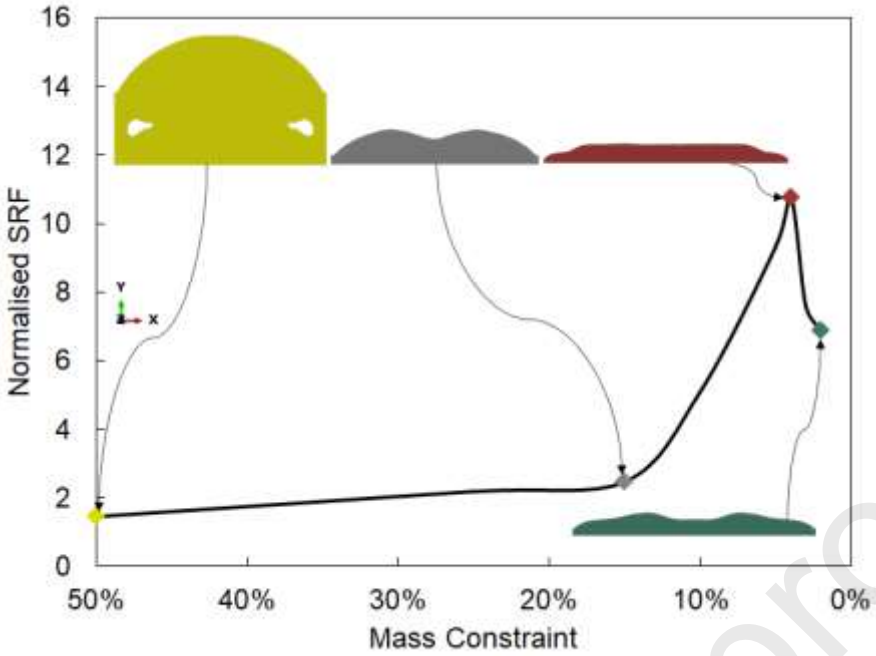

Figure A.4 Different designs and performance of the TOP process